International Symposium of Research Students on Materials and Engineering

December 20-22, 2004, Chennai, India

Department of Metallurgy and Materials Engineering, Indian Institute of Technology Madras

Al-BASED NANOCOMPOSITES BY NON-EQUILIBRIUM PROCESSING ROUTES

S. S. Nayak [1, 2], D. H. Kim [2], S. K. Pabi [1] and B. S. Murty [3]

[1] *Indian Institute of Technology, Kharagpur 721 302, India*

[2] *Center for Noncrystalline Materials, Yonsei University, Seoul 120-749, South Korea*

[3] *Indian Institute of Technology, Madras, Chennai 600 036, India*

ABSTRACT

Successful synthesis of Al-based nanocomposites by mechanical alloying (MA) and rapid solidification processing (RSP) with functional mechanical properties, in Al-Fe and Al-Ti systems, has been reported in the present paper. In melt spun Al-Fe ribbons fine cellular structure, dendritic structure, fine dispersion of second phase particle and particle segregations at α-Al gain boundaries were observed depending on compositions. Whereas, in Al-Ti system only a two phase mixture forms irrespective of the composition. However, volume fraction of $L1_2$-Al_3Ti precipitates in Al-Ti alloys is more in as spun ribbons compared to MA powders. MA shows improved hardness value, which further increases with annealing temperature.

1. INTRODUCTION

Benjamin group[1] has led to the evolution of mechanical alloying (MA), a solid state synthesis route which, apart from equilibrium phases produces non-equilibrium phases like amorphous phase. Since then MA has attracted lot of interest of materials scientists to produce both stable and metastable phase.[2] Previously effective synthesis of Al alloys containing significant amount of ultrafine Al_4C_3 and Al_2O_3 dispersoid[3] which contributes mainly to the high temperature strength of MA alloys. Properties of such Al alloys can be enhanced by the addition of Al-TM (transition metals) intermetallics. When we talk about the Al-TM systems, the main binary systems that come into picture are Al-Fe, Al-Ti and Al-Zr binary alloy phase diagrams. The alloys and intermetallics of these binary systems are attractive for application at temperatures beyond those normally associated with Al alloys use. Alloying aluminum with iron increases the high temperature strength due to dispersion of second phase particles, [4] but the main disadvantage is the limited solubility of Fe in Al which is 0.03at.% at high temperature. Hence, Al-Fe alloys cannot be dispersion strengthened with conventional heat treatment. This can be

overcome by extending the solubility limit of Fe in Al, which has been reported to be achieved by non-equilibrium processing techniques like MA[5] and/or rapid solidification processing[6] (RSP) which produces materials in nanocrystalline state alongwith dispersion of metastable phases.

As compared to other Al rich intermetallics, Al_3Ti is very attractive because of its high melting point (~1350C) and lowest density of ~3.3 g/cm^3. Further, Ti has low diffusivity and solubility in Al, hence Al_3Ti is expected to exhibit low coarsening rate at elevated temperature. According to the characteristics of the microstructure, MA of Al-Ti alloy may be considered as a fine Al-Al_3Ti two-phase composite. By non-equilibrium processing technique like MA and RSP, Al-Al_3Ti composites with different volume fraction of Al_3Ti reinforcement alongwith other metastable phase can be produced. Also the other microstructural factors such as size, amount and distribution of fine dispersions of intermetallic phases as well as the grain size of Al matrix can be maintained. Therefore, Al-Al_3Ti prepared by non-equilibrium processing routes can serve as a good candidate material for structural applications.

2. EXPERIMENTAL DETAILS

Elemental blends were mechanically alloyed in a high energy planetary ball mill (FRITSCH P5) at 300rpm with ball to powder ratio of 10:1. The MA powders were consolidated into pellets of Ø12mm and 5mm height to yield about 90% of theoretical density under load of 5.5Tons (375MPa) using uni-axial hydraulic press. Melt spinning (RSP) of the mother alloys, prepared by induction melting of high purity elements, was carried out with a linear wheel speed of 40ms^{-1}. Melt spun ribbons were 2-4mm wide and 30-80μm thick. Phase analyses of both MA powders and melt-spun ribbons were carried out by X-ray diffraction (XRD). The crystallite size of the milled samples was calculated from XRD peak profile using Voigt analysis.[7] Microstructures of as spun ribbons have been investigated by transmission electron microscopy (TEM) using JEOL JEM 2000EX electron microscope. Microhardness was measured under a load of 10gm and 300gm for ribbons and pellets respectively. The thermal analysis was carried out by differential scanning calorimeter (DSC).

3. RESULTS AND DISCUSSION

In the present paper, the sequence of presenting the results and discussion will be is; Nanocomposites by MA→ Nanocomposites by RSP→ Comparison of MA and RSP (includes structural evolutions and mechanical properties)

3.1 Nanocomposites by mechanical alloying (MA)

3.1.1 Al-based nanocomposites with Al_3Fe precipitates

The structural evolution of Al-Fe alloys after 20h of MA is shown in Fig. 1(a). Formation of single phase of Al(Fe) solid solution was observed in all the compositions studied except the 20% Fe containing alloys. As the Al(200) and Fe(110) peaks are observed at same diffraction angle it was thought to measure the ratio of relative intensities of Al(111) and Fe (110) peaks after 20h of MA. The measured values were plotted against the Fe content in the alloys and it was found to follow as straight line as shown in Fig. 1(b). This shows that the richer the alloy with iron, the lower the intensity Al(111) peak suggesting that at extrapolation of the composition to 25%Fe (where the single phase Al_3Fe forms) should bring the ratio down to zero. The crystallite size was calculated to be less that 20nm irrespective of the composition.

Annealing above 473K, the XRD plot (not shown in figure) of the pellets forms nanocomposites with persistence of nanocrystallinity of both α-Al matrix as well as the dispersed Al_3Fe phase. Particularly the $Al_{80}Fe_{20}$ composition shows the formation of Al_5Fe_2 intermetallics with very low volume fraction of α-Al after 20h of MA, as seen from XRD plots in Fig. 1(a). Interestingly, after annealing unlike other compositions it dissolved the α-Al into the intermetallics and resulted in formation of new single phase Al_3Fe intermetallic (not shown in figure).

3.1.2 Al-based nanocomposites with $L1_2$-Al_3Ti precipitates

XRD patterns (not shown in figure) of the MA powders shows the broadening of the Al peaks along with shift towards the higher angle showing formation of nanocrystalline (less than 30nm) solid solutions of Ti in Al. After 20h of MA, significant change in lattice parameter of the Al from 0.4050nm to a value 0.4028nm was observed. 1at.% Ti contracts the Al lattice by 0.001nm. Hence the present result suggests that MA has enhanced solubility of Ti in Al to a level of around 2.2 at.%. From the change in lattice parameter of Al with composition as well as duration of MA suggest that supersaturated solid solution has been formed rather only solid solution in all the compositions studied in the present work. DSC of MA powders was carried out at a heating rate of 40K/min starting from room temperature to 700^{o}C to know the temperature of precipitation of $L1_2$ phase. DSC traces show exothermic peaks in the range of temperature 350 to 450^{o}C, which signifies the precipitation of $L1_2$-Al_3Ti phase.

The XRD patterns of binary Al-Ti compositions annealed at 400C (673K) are shown in Fig. 2(a). Precipitation of $L1_2$ phase has been observed to have a shoulder peak coming of the Al(111) peak in almost all the composition. Fig. 2 (b) shows the variation of hardness with composition

as well as temperature of annealing respectively for $Al_{100-X}Ti_X$ nominal composition. Almost 96% of theoretical density has been observed after annealing at 673K. Hardness increases with increase in solute content and also with the increase in annealing time keeping the same annealing time. Highest hardness value achieved in Al-Ti systems was found to be 3.5GPa. As empirically yield strength is one third of the hardness value, yield strength of around 1.2GPa can be expected to achieve in the present Al-Al_3Ti nanocomposites.

3.2.0 Nanocomposites by melt spinning (RSP)

3.2.1 Al-based nanocomposites in Al-Fe system

Fig. 3 shows the XRD patterns of $Al_{100-X}Fe_X$ (x=2.5, 5, 10, 15 and 20). Formation of intermetallics like Al_5Fe_2 and $Al_{13}Fe_4$ are clearly evident from it. Also the presence of partial amorphous phase in the higher Fe containing alloys such as Al-10%Fe and 15% Fe alloy was observed. All the compositions studied form nanocomposites of Al and intermetallics except the 20%Fe containing alloys, which forms monoclinic $Al_{13}Fe_4$ intermetallics. The volume fraction of the second phase particles were very less and the peaks of them were observed to merge with that of Al(200) peak, hence making it difficult to confirms the presence of a particular intermetallics. Also in Al-Fe phase diagram intermetallics with very complex crystal structures are formed with most of the intermetallics giving their most intense peaks at the same diffraction angle as Al(200) peaks hence the difficulty to confirm it by XRD. However, TEM study could confirm the presence of complex Al-Fe intermetallics.

3.2.2 Al-based nanocomposite in Al-Ti system

Melt spinning at 40m/s speed of the $Al_{100-X}Ti_X$ (x = 5, 10, 15 and 20) formed Al-based nanocomposites with very fine embedded metastable $L1_2$-Al_3Ti phase with sufficient volume fraction as shown in Fig. 2(a). The volume fraction of $L1_2$ phase increases with Ti content in the composition. Interestingly, 20%Ti containing alloy forms nanocomposite with precipitates of equilibrium DO_{22} structure of Al_3Ti intermetallic.

Hardness value of the nanocomposites was found to increase with Ti content (Fig. 2 (b)) in the alloy up to 15%Ti containing alloy. It is due to the increase in volume fraction of dispersed $L1_2$-Al_3Ti phase as clearly seen from XRD pattern in Fig. 2(a).

3.2.3 Comparison of MA and RSP

3.3.1 Microstructural evolution

In melt spun Al-Fe alloys, metastable phases like mico/nano quasicrystals, Al_5Fe_2, $Al_{13}Fe_4$, Al_3Fe form depending on the composition. All the metastable phases form either as micro cellular structure, dendritic structure, and fine dispersion of second phase particle or as segregated particles at α-Al gain boundaries.

Fig. 5(a) shows presence of bright nano quasicrystals with average size of 10nm giving rise to diffraction rings along with the diffraction spots of Al matrix with [110] zone axis. MA, unlike RSP, did not form any metastable phases but forms solid solution and equilibrium Al_5Fe_2 intermetallic. Fig. 5(b) shows the bright field image of melt spun Al-5%Ti alloy at a speed of 40m/s. This shows the formation of a mixture of two phases namely $L1_2$-Al_3Ti precipitates and Al matrix. The dark areas seen in image are $L1_2$ particles dispersed uniformly in bright Al matrix. SAD pattern taken from one of the dark particle confirms the presence of fcc $L1_2$ structure of Al_3Ti phase.

3.3.2 Mechanical properties

Hardness can be termed as a measurement of mechanical properties of the nanocomposites. The plots in Fig. 6(a) and (b) show the variation of hardness of pellets prepared from MA powder and melt spun ribbon of Al-Fe alloys respectively. It is quite easily observed that the hardness of MA alloys increase with increase in Fe content as well as annealing temperature. 20%Fe containing alloy measures a hardness value of 12.2GPa, which is highest ever reported value for any Al alloys. The melt spun ribbons shows lower hardness value compared to nanocomposites prepared by MA. This can be attributed to several defects being incorporated in MA powders which enhances the hardness and mechanical properties of the nanocomposite. Hence it is concluded that MA enhances the mechanical properties of the materials compared to melt spinning (RSP). Also it was seen from present work that hardness and hence mechanical properties of nanocomposites get enhanced with more solute content and also by increasing the temperature of annealing till 673K irrespective of the binary systems studied.

4. CONCLUSIONS

1. MA of Al-Fe results in the formation of nanocrystalline supersaturated solid solution where as melt spun Al-Fe alloys form metastable phases like micro/nano quasicrystals, Al_mFe, Al_5Fe_2 or $Al_{13}Fe_4$ depending on their thermodynamic stability.
2. Nanocomposites containing $L1_2$-Al_3Ti, with a high hardness value of 3.5GPa and empirical yield strength of 1.2GPa, have been successfully synthesized both by MA + annealing and melt spinning of binary Al-Ti compositions.

3. Hardness increases with increasing solute content and annealing temperature irrespective of the alloy system.
4. MA is better enhancer of the mechanical properties as compared to melt spinning though both are non-equilibrium processing techniques.

ACKNOWLEDGEMENT

The author S. S. Nayak a Senior Research Fellow (SRF) of CSIR, New Delhi, is thankful to the organisation for the financial support to carry out the research work

REFERENCE

1. Benjamin J S, *Met Trans* **1** (1970) 2943.
2. Murty B S, and Ranganathan S, *Int Mater Rev* **43(3)** (1998) 101.
3. Suryanarayana C, *Prog Mater Sci* **46** (2001) 1.
4. Kim YW, in KimYW and Griffit WM (eds): *Dispersion strengthened aluminium alloys*, The Metallurgical Society, Warrendale, PA, 1988.
5. Tonejc A, and Bonefacic A, *J Appl Phys* **40(1)** (1968) 419.
6. Mukopadhyay DK, Suryanarayana C, and Froes FH, *Metall Mater Trans A* **26A** (1995) 1939.
7. de Keijser TH, Langford JI, Mittemeijer EI, and Vogels A B P, *J Appl Crystallogr* **15** (1982) 308.

FIGURES

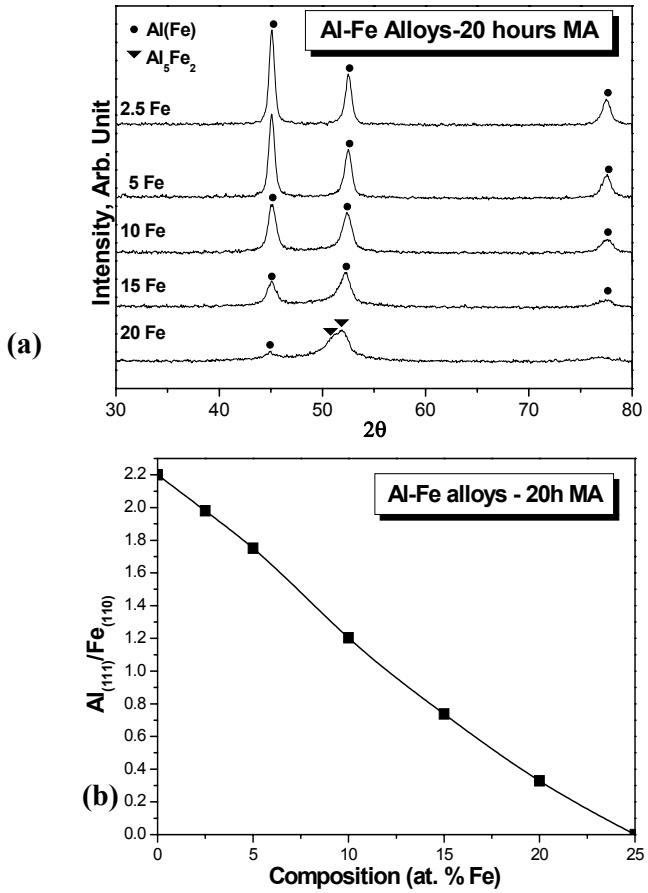

Fig. 1 (a) XRD patterns of Al-Fe alloys after 20h of MA, (b) intensity ratio of Al(111) and Fe(110) with Fe content in the alloys.

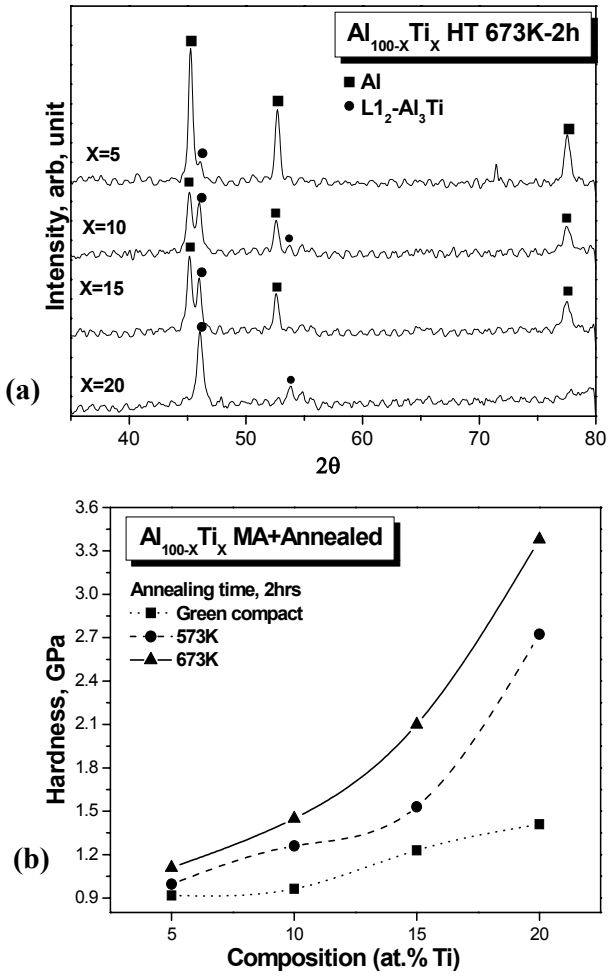

Fig. 2 (a) XRD pattern of nanocomposites in Al-Ti binary system, (b) variation of hardness with annealing temperature and alloy composition.

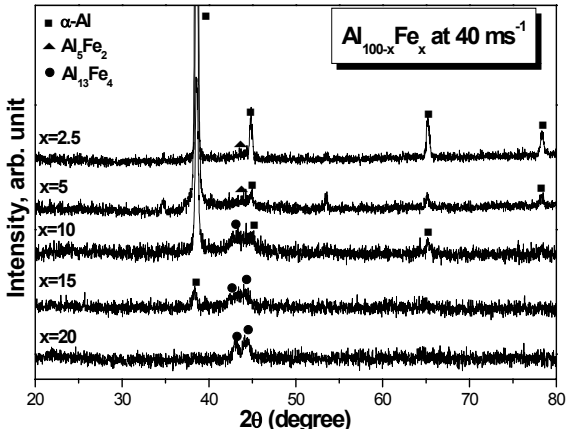

Fig. 3 XRD of Al-Fe alloys melt spun at 40m/s.

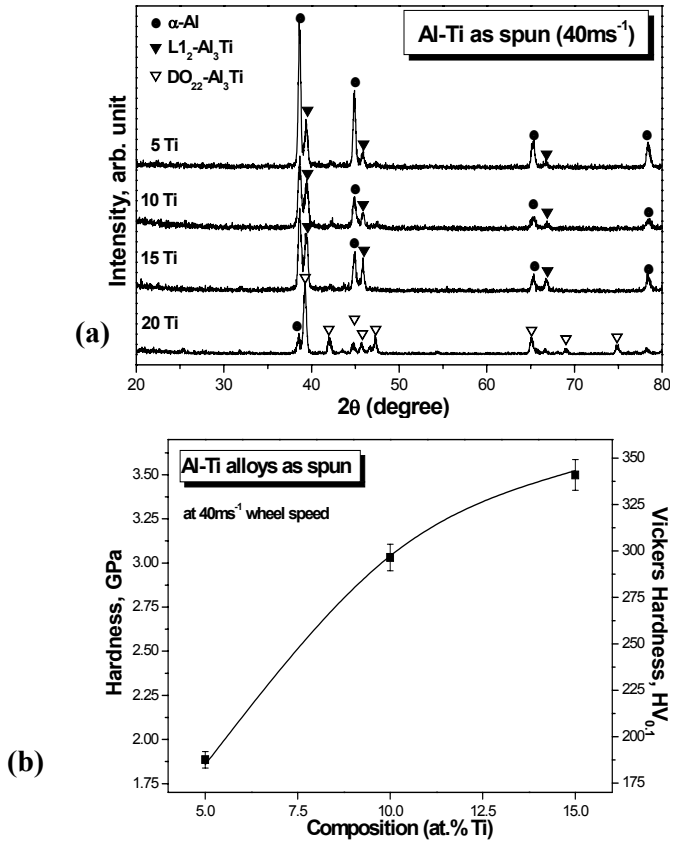

Fig. 4 (a) XRD of Al-Ti alloys melt spun at 40m/s, (b) variation of hardness with compositions of melt spun Al-Ti alloys.

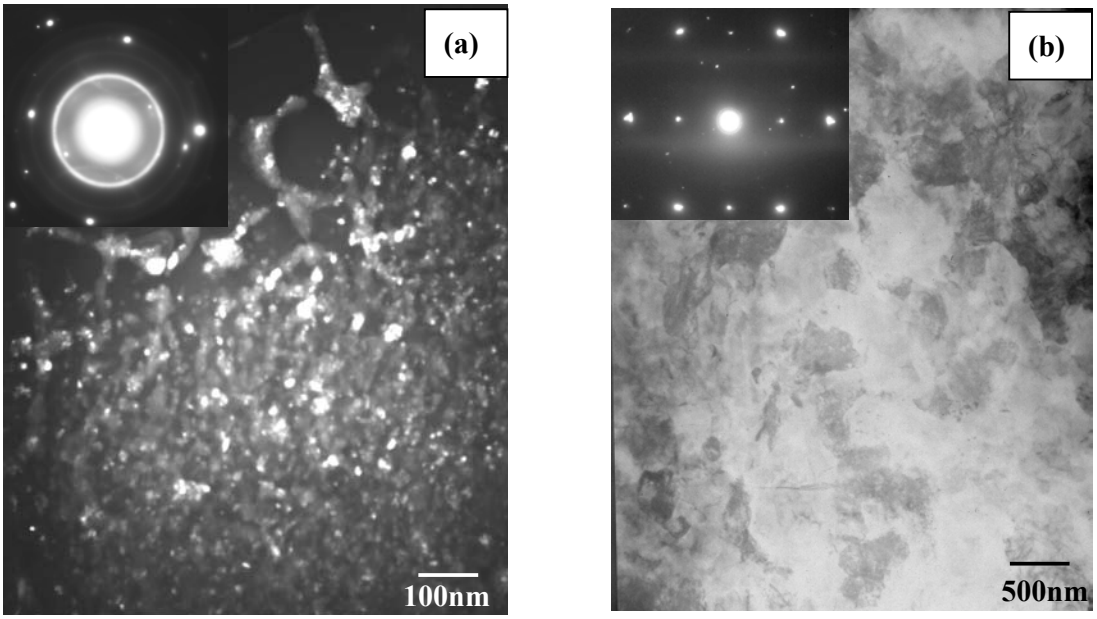

Fig. 5 (a) Dark field image of Al-2.5Fe alloy melt spun (40m/s) insert is SAD pattern, (b) Bright field image of Al-5Ti alloy melt spun (40m/s) insert is the SAD pattern of the dark $L1_2$ particle.

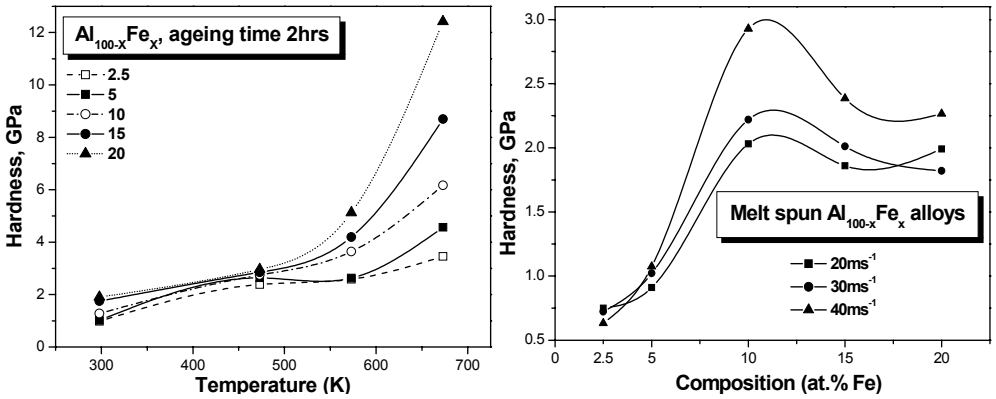

Fig. 6 Variation of hardness of Al-Fe alloys with composition (a) annealing temperature and (b) melt spinning speed